PFC/JA-96-31

Pyrometry Inside an Arc Furnace Using a Ray-Tracing Correction for Surface Emissivity

S.K. Lee and P.P. Woskov

October 1996

Plasma Fusion Center
Massachusetts Institute of Technology
Cambridge, MA 02139

Submitted to *Journal of Computer-Aided Materials Design*

Supported by Battelle - Pacific Northwest National Laboratory as part of the Landfill Stabilization Focus and Mixed Waste Areas, Office of Technology Development, Environmental Management, U.S. Department of Energy.

Pyrometry Inside an Arc Furnace Using a Ray-Tracing Correction for Surface Emissivity

Sang Kook Lee and Paul P. Woskov

Plasma Fusion Center, Massachusetts Institute of Technology, Cambridge, MA 02139

SUMMARY

A general method using a ray-tracing analysis has been developed to improve the accuracy of surface temperatures measured by pyrometry inside a furnace. This method allows temperature correction for enclosed non-ideal black-body surfaces, having temperature gradients, by taking into account the contributions from the reflected fraction of the pyrometer field-of-view. The development has been made possible by the recent availability of internal furnace scanning pyrometry technology for complete temperature profile measurements inside furnaces. The correction method can be expressed in terms of the solution of a square matrix having a dimension corresponding to the number of spatially resolved points in the temperature profile with the number of non-zero elements depending on the number of field-of-view reflective surface bounce points used in the analysis. The utility of this method is demonstrated for correction of 19 point temperature profiles measured inside a dc arc furnace. Reflective contributions from two, three, and four field-of-view surface bounce points are considered. Generally, the lower the surface emissivity and the higher the temperatures, the more bounces need to be included in the analysis. It is shown that there can be significant corrections to internal furnace temperatures measured by pyrometry when temperature gradients exist.

1. INTRODUCTION

High temperature processes are important in the manufacture of many materials including glass, ceramics, semiconductors, composites, and in metal refining, casting, and annealing to name a few. In addition, high temperature processes are used for waste remediation and for power production. In all these processes temperature is the most fundamental parameter which must be monitored to insure that a quality product is produced. Furthermore, in many of these processes only non-contact measurements can be used in order to avoid contamination or damage to the product, to avoid a contacting safety hazard or temperature limit, to maximize time response, or because the product is moving.

Non-contact temperature measurements are generally accomplished using pyrometer instrumentation, which can remotely detect the electromagnetic thermal emission characteristic of all bodies. A major difficulty with this approach is that most surfaces that need to be monitored are not ideal black-body emitters. Their surface emissivities are less than one and can change during the process. A part of the pyrometer field-of-view is generally reflected or transmitted to view other surfaces when the emissivity of the target surface is less than one. Consequently assigning a temperature to the target surface due to the measured thermal emission can be challenging. This has stimulated much work to develop specialized instrumentation and analytic interpretations to make possible accurate pyrometric temperature measurements.

One method to deal with unknown emissivity is two color pyrometry. The slope of the black-body emission spectrum at two fixed wavelengths on the high frequency side of the spectrum can be used to obtain a temperature without knowledge of the emissivity as long as the emissivity is identical at both monitored wavelengths. This is a common pyrometry method which has recently been applied to molten uranium metal in casing furnaces [1] and to glass slag in a plasma melter

for vitrification of high level nuclear waste [2]. However, the fundamental assumption that the emissivity at the two monitored wavelengths is exactly the same can not always be guaranteed.

Another approach is to control the reflected component of the field-of-view (FOV) either by trapping it or directing it to a controlled location. Trapping the pyrometer FOV with a conical cavity has been applied to temperature measurements of sheet steel in a continuous annealing furnace [3]. Orientating the pyrometer FOV normal to the monitored surface to return the FOV reflection to the pyrometer has been applied to architectural glass manufacture [4]. This approach is generally limited to optically smooth surfaces with normal FOV access, and in the case of trapping cavities to clean environments of not too high temperature where a highly reflecting cavity can be implemented.

Careful analytical interpretation of the pyrometer signals have also been developed which take into account all the possible spurious contributions which can mask the desired surface temperature measurement. Such analyses have been developed for optical furnaces used to radiatively heat ingots [5] and for radiatively heated furnaces used in semiconductor integrated circuit manufacture [6]. Some approximations must always be made in these analyses about radiative contributions from the surrounding environment.

In the work presented here we take advantage of a new pyrometer technology, the active millimeter-wave pyrometer [7], which allows the scanning of complete temperature profiles inside harsh high temperature environments along with a capability for simultaneous measurement of the surface emissivity of appropriately aligned surfaces. Sufficient information can be obtained by this single wavelength pyrometer to accurately determine non black-body surface temperature profiles inside an enclosed furnace environment. We can quantitatively determine the contribution

from other surfaces to the target surfaces signal which to date could only be approximated, for example, by terms such as the veiling glare term of reference 6.

The analysis consists of two main parts [8]. First, the reflected component of the pyrometer FOV is traced to identify the surface points that contribute to the pyrometer signal for each direction viewed in the profile scan. Generally we find here that only up to four reflective bounce points need to be considered for emissivities down to 0.7. Second, an emissivity matrix is set up which is a square matrix with a dimension corresponding to the number of points in the measured temperature profile. The number of non zero elements in this matrix depends on the number of reflective bounces considered in the analysis. A measured temperature profile is readily converted to an actual temperature profile by multiplication with the inverse of this emissivity matrix.

The analysis is carried out for actual temperature profile measurements made in the Mark II dc graphite electrode arc furnace at the MIT Plasma Fusion Center. This is a pilot scale furnace being evaluated for the treatment of mixed wastes in the DOE complex [9]. A rotating graphite waveguide with a graphite miter mirror [10] was used to obtain complete vertical profiles of the thermal emission at a frequency of 135 GHz. Temperature gradients were found to exist under all operating regimes of the furnace so that the analysis as developed here is necessary to obtain the highest possible temperature measurement accuracy.

This is a general method which can be applied to any high temperature process with a well defined internal boundary. It also could be used with IR as well as with millimeter-wave pyrometers. However, specular reflections for ray tracing, robust high temperature scanning optics, and simultaneous measurements of emissivity are much more readily accomplished at millimeter wavelengths. The application of this technique to more accurate temperature measurements should make possible a new degree of control for improved productivity in the manufacture of many currently

available materials, as well as, make possible the development of new and more advanced materials.

2. TEMPERATURE CORRECTION METHOD

a. Theoretical Background

It is well known that in the long wavelength range of the black-body emission spectrum were the Rayleigh-Jeans approximation is valid that there is a linear relationship between temperature T, and the emitted thermal electromagnetic power, P, [11-13] which in this case can be expressed as

$$P = k_B \varepsilon T \Delta f, \tag{1}$$

where k_B is the Boltzmann constant, Δf is the frequency bandwidth over which the signal is detected, and ε is the surface emissivity. As long as the surface at temperature T fills the millimeter-wave pyrometer FOV the signal detected will be given by Eq. (1). In the following, the analysis will be developed in terms of temperature and emissivity which through Eq. (1) correspond to the actual signal levels detected.

When the emissivity is less than one a fraction of the pyrometer FOV corresponding to (1-ε) sees another surface, and if that other surface has an emissivity of less than one then a fraction of the original fraction of the pyrometer FOV sees yet another surface and so on with diminishing signal contributions from subsequent surfaces. For the first few terms this can be expressed as:

$$T_1^m = \varepsilon_1 T_1 + (1-\varepsilon_1)\varepsilon_2 T_2 + (1-\varepsilon_1)(1-\varepsilon_2)\varepsilon_3 T_3 + \ldots, \tag{2}$$

where we have designated the raw measured temperature signal with a superscript m and the successive surface bounce points for the pyrometer FOV with numerical subscripts. The first term on the right is the thermal signal for the desired target surface. The following terms are the contributions to the measured thermal signal from other surfaces. The lower the surface emissivities the more terms need to be included. Equation 2 can be generalized by the expression:

$$T_1^m = \sum_{n=1}^{\infty}\left[\prod_{l=0}^{n-1}(1-\varepsilon_l)\right]\varepsilon_n T_n \quad , \qquad \varepsilon_0 = 0 \, . \tag{3}$$

Generally only the first few terms of this equation are needed for most practical cases.

The work presented here is basically the solution of a set of Equations (3), one for each point in the measured temperature profile, to obtain the actual temperatures, T_n, inside the furnace.

b. Assumptions

Three assumptions were made in the present analysis. First, it was assumed that treating the millimeter-wave FOV beam as a single ray is valid. Strictly speaking the millimeter-wave FOV is a diverging Gaussian beam [10]. However, this assumption is justified because the temperature gradients inside Mark II are smoothly varying and a ray centered on the FOV spot would be representative of the average thermal signal in the whole spot. For the total FOV propagation distances considered here, up to four reflective bounces, the spot size is generally much smaller than the internal dimensions of the furnace.

Second, cylindrical symmetry was assumed to obtain a 3-dimensional picture of the temperature gradients. This assumption is justified because the arcing electrodes are a coaxial pair running down the center of the cylindrical furnace with

the arc heating occurring in the center of the hearth [9]. This assumption was also necessary because the vertical scan of the temperature profile was not made in the longitudinal midplane of the furnace so that knowledge of the out-of-plane temperature gradients was needed for this analysis.

The third assumption was that the surface emissivity is uniform inside the furnace. Equation 3 thus simplifies to:

$$T_1^m = \sum_{n=1}^{\infty} \varepsilon(1-\varepsilon)^{n-1} T_n = \varepsilon T_1 + \varepsilon(1-\varepsilon)T_2 + \varepsilon(1-\varepsilon)^2 T_3 + \cdots, \qquad (4)$$

where ε is the emissivity everywhere inside the furnace. The basis for this assumption is the observation that the internal furnace surface is uniformly coated with the slag material after a furnace run. In this case the assumption of uniform emissivity at one wavelength is more likely to be correct than the assumption of equal emissivity at two different wavelengths made for two color pyrometry. However, this analysis can be generalized to non uniform emissivities. As an example we will also consider here an emissivity in the hearth which differs from the rest of the furnace walls.

c. Analysis Method

i. Ray Tracing

The first step in the analysis method is to determine the surface locations that the reflected part of the pyrometer FOV intersects as it bounces around inside the furnace. A set of bounce locations must be determined for each viewed direction in the profile scan. This is accomplished by geometrical ray tracing using the rule that the FOV angle of reflection is equal to the angle of incidence relative to surface normal at each reflection. For high surface emissivities (≥ 0.9) and low temperatures only one reflection (two bounce points) are sufficient for the analysis. For

emissivities down to 0.7 and high temperatures we show here that three reflections (four bounce points) are sufficient.

The ray tracing procedure can best be described by considering an example. We use the active millimeter-wave pyrometer set up on the Mark II arc furnace. Figure 1 shows an elevation view of the cylindrical Mark II furnace in the pyrometer FOV launch plane. The rotatable waveguide with a miter mirror allows vertical profile measurements as shown. In the present case the vertical profiles consist of 19 point measurements taken at 10° rotation increments of the waveguide with 0° designated as viewing approximately straight up and 180° as viewing straight down. The analysis could be readily extended to include more points in the profile.

The internal diameter of Mark II is 91.9 cm with a height of 109.2 cm from the top of the slag surface. The pyrometer waveguide enters the furnace 69.2 cm above the slag surface and the center of the FOV protrudes 6.4 cm into the furnace from the side wall. The slag height in Mark II remains approximately constant during operation because the slag is poured by overflowing into a spout as waste is fed into the furnace. The coaxial central electrodes that occupy the inner 42 cm diameter of Mark II do not need to be included in the ray tracing analysis because the reflected parts of the FOV do not pass through that region. However, the ray tracing analysis could easily be extended to include electrodes and other objects that could reflect the pyrometer FOV inside the furnace.

The ray tracing analysis is illustrated in Figure 2 for the 50° initial viewing direction. It is convenient to carry out this analysis in Cartesian coordinates and then convert the reflection location to cylindrical coordinates for formulating the emissivity matrix below. The determination of the reflective bounce points as shown in Figure 2 is carried out for each pyrometer view direction. For the special cases of viewing straight up or down, when the reflection is directed back to the pyrometer, we assume the FOV passes by the launch mirror to the opposite

surface. This assumption is justified because the FOV is diverging as it propagates and only a small part of the return reflection is blocked by the launch mirror.

ii. Emissivity Matrix

Once all the surface bounce point locations have been determined the temperatures at those locations must be expressed in terms of the initially viewed points in the temperature profile, i.e., the 19 points in the Mark II profiles, T_0, T_{10}, T_{20}, ·····, T_{180}. This is necessary to reduce the number of unknown temperatures in the set of equations, each given by Eq. 4 of the profile scan. In the case of Mark II temperature profiles this will result in 19 equations and 19 unknowns.

The number of unknown temperatures is reduced by interpolating the temperature at the surface locations between the initially viewed points in terms of T_0, T_{10}, T_{20}, ·····, T_{180}. For the points that fall outside the plane of the profile scan on the ceiling and slag surfaces we assume a linear extrapolation of the temperature gradient to radial dimensions not scanned in the initial view. In some cases when the FOV bounce point is very close to an initially viewed location, less than the FOV spot size, the temperature can be taken to be the same as the adjacent first bounce location.

An illustration of the resulting equations is given in Table 1 for the Mark II furnace case considering only one reflection (two surface bounce points). The first column lists the initial view direction in the profile scan (as shown in Figure 1). The second column gives the location of the first surface viewed in cylindrical coordinates. For r=45.7 cm the location is on the side wall and for z=0, 109.2 cm the location is on the slag surface and the ceiling, respectively. The second column is the location of the second bounce point. The final column lists the raw measured temperature in terms of the actual surface temperature to be determined. The first term on the left side of these equations corresponds to the T_1 term in Eq. 4

and the following terms correspond to the T_2 term. The T_2 term has been interpolated between two initially viewed surface temperatures when the second bounce point occurs between these points. For the special case of the 90° view, when the FOV reflections remain in the same azimuth, the measured temperature has been set equal to the actual temperature due to the cylindrical symmetry assumption.

The equations of Table 1 are to put together to form the emissivity matrix which is used to find the corrected temperatures as a solution set. Each equation is expanded to include all initially viewed temperatures with the additional terms having zero valued coefficients. This set of equations can then be written as

$$E\vec{x} = \vec{b}\,, \tag{5}$$

where E is the 19 by 19 coefficient matrix expressed in terms of emissivities, $\vec{x} = (T_0, T_{10}, T_{20}, \cdots, T_{180})$ is 1 by 19 column matrix which we want to find, and $\vec{b} = (T_0^m, T_{10}^m, T_{20}^m, \cdots, T_{180}^m)$ is 1 by 19 column matrix which represents the experimentally measured raw temperatures.

Once all the measured temperatures and the emissivity are known, the corrected temperatures are found by the inverse of the emissivity matrix operation.

$$\vec{x} = E^{-1}\vec{b}\,. \tag{6}$$

Many popular programs are available which can be used to readily solve Eq. (5). Here we use Microsoft EXCEL. Figure 3 illustrates the solution of the set of equations given in Table 1 for the simplest case of one reflection (two surface bounce points). The surface emissivity has been made equal to 0.74, a value determined to be representative of the Mark II furnace slag coated walls. The 19x19 matrix represents the coefficients of the equations given in Table 1. In general, the diagonal elements

correspond to the first surface bounce point and the off-diagonal elements represent contributions to the signal from the second surface bounce point. The one exception in the example given in Figure 3 is the diagonal element for the initial view direction of 150° where the interpolated second bounce temperature also includes a component from the 150° first bounce location. If more than one reflection of the pyrometer FOV is included in the analysis then more of the off-diagonal elements would be non zero. Once the emissivity matrix is set up the measured temperature profile can be entered into the software, as illustrated by the first column to the right of the matrix in Figure 3, and automatically converted to a corrected temperature profile as shown by the last column.

The solution of Eq. (5) is a very powerful tool. It can be adapted to larger or smaller temperature profile data sets, poly-emissivity cases, or temperature profiles that are measured at irregular intervals. In many cases once the emissivity matrix is determined, for a given furnace geometry and number of temperature profile scan points, it will remain the same for most, if not all, furnace operations. Raw temperature profiles could be corrected in near real-time by entering them into the computer as they are measured. The surface emissivity could also be updated in real time if a pyrometer with active probing is used to determine this parameter.

3. RESULTS AND DISCUSSION

a. Uniform Surface Emissivity

The ray tracing and emissivity matrix temperature correction method was applied to actual temperature profiles taken inside the Mark II arc furnace. The effect of including one, two, or three reflections of the pyrometer FOV in the analysis is shown for a low temperature profile (100 - 500 °C) in Figure 4 and a high temperature profile (1200 - 1500 °C) in Figure 5. The lower temperature profile was taken during furnace warm up and the high temperature profile corresponds to when the furnace

was at temperature for soil melting operations. The emissivity of the internal furnace surfaces for this data was estimated from the active millimeter-wave pyrometer measurements at representative wall and ceiling surfaces to be approximately 0.74 ±0.03 at 135 GHz [7].

Including only one reflection (two surface bounce points) in the analysis for Mark II is not sufficient. This is evident in both Figures 4 and 5 because including another reflection in the analysis, by going to three surface bounce points, makes a significant change in the resulting temperature profile. In addition, there is a discontinuity in the corrected profile at the 90° view angle, a consequence of our cylindrical symmetry assumption, which is particularly evident in Figure 5. There is no physical basis for such a temperature dip at this location or for the temperature to be increased everywhere else across the profile. A valid correction to the temperature profile should include all significant higher order terms due to higher order reflections and make intuitive sense.

Two reflections (three surface bounce points) must be included in the analysis for the lower temperature profiles and three reflections (four surface bounce points) for the higher temperature profiles. With these additional reflections included the corrected temperature profiles are seen to converge to a result without any unrealistic discontinuities. The dip in the plots at 50° view angle corresponds to the corner where the ceiling and wall meet. More terms are needed at higher temperatures because the magnitude of higher order terms in Eq. (4) increases with temperature as well as with lower emissivity.

The resulting corrected temperature profiles make intuitive sense. The effect of the correction is to increase the overall temperature gradient between the hottest areas in the hearth (150° to 190° view direction) and the coolest areas on the ceiling (0° to 50° view direction). This is to be expected because when viewing into the hottest region of the furnace the reflective contributions to the resulting signal are

from cooler regions so the correction increases the measured temperature. Conversely, when viewing the coolest region of the furnace the reflective contributions are from hotter regions and the correction decreases the temperature. In fact, the correction is largest for the hearth and ceiling temperatures because the opposite extreme in the temperature gradient is viewed on first reflection, the largest contributing term to the correction. The corrections to the intermediate temperatures on the wall surfaces are much smaller because the first reflective contributions are from nearby surfaces with similar temperature.

The largest correction is for the temperature of the slag in the hearth. This generally is the most important temperature for monitoring and controlling a furnace process. If the material in the furnace is not heated to the correct temperature a deficient product might result or the viscosity may not be correct for pouring. The error in the raw measurement of slag temperature in Mark II by millimeter-wave pyrometry, if the ray-tracing and emissivity matrix correction is not applied, is approximately 4% or 60 °C too low at about 1400 °C for the high temperature profile of Figure 5. The viscosity of glass produced from soil changes rapidly with temperature in this range and a 60 °C error in temperature is significant. It is therefore important to use the temperature correction method as developed here.

The error in the raw temperature measured by pyrometry depends on the overall temperature gradient inside the furnace as well as on the surface emissivity. For larger temperature gradients as during furnace warm up as shown in Figure 4, the corrected temperature at the slag surface is 17% higher than the uncorrected measurement. The effect of different uniform surface emissivities on the temperature correction is shown in Figure 6 for the high temperature profile data. As the emissivity is decreased form 0.9 to 0.8 and 0.7, the error in the slag temperature increases from 1% to 3% and 6%, respectively. As expected the needed correction in the raw data increases as the surface emissivity deviates more from the ideal black-body value of 1.0.

It is interesting to note that the corrections to the raw temperature measurements by pyrometry inside a furnace are much smaller than a simple compensation for the surface emissivity as would be done for an unenclosed heated surface. The usual correction to a pyrometric temperature measurement of an unenclosed surface is to multiply the raw measurement by ε^{-1}. In the present case for a surface emissivity of 0.74 that would increase the raw temperature by 35%. The analysis presented here shows that this would be an incorrect approach for heated surfaces enclosed by other heated surfaces. It could cause greater errors than not correcting the data at all for surface emissivity. The actual correction for surface emissivity inside a furnace is a value that falls between ε^{-1} and 1.0. This value can be analytically determined by the ray tracing and emissivity matrix treatment presented here.

b. Non-Uniform Surface Emissivity

The ray tracing and emissivity matrix correction method can be readily adapted to non-uniform surface emissivity inside the furnace. We illustrate this by considering a case were the surface emissivity of the slag differs from the rest of the internal furnace surfaces. This situation is probably representative of many applications of high temperature processing. For example, in the aluminum industry the molten electrolyte used in reduction pots for the production of aluminum can be highly conductive and thus have a much lower emissivity than the surrounding enclosure surfaces.

In Figure 7 the high temperature Mark II profile data is reevaluated with the assumption that the slag surface emissivity is 0.3 and 0.5 with the rest of the surfaces at 0.74. The main difference relative to the uniform emissivity case is that the slag surface temperature correction is now much larger. This can be easily understood as a lower surface thermal radiated power due to the lower surface emissivity causing the

pyrometer to underestimate the actual surface temperature by a larger degree. The other surface regions including the cold ceiling and the wall surfaces have temperature profiles that are very similar to the uniform emissivity analysis, with the temperature corrections becoming even smaller as the slag surface emissivity decreases. This can be understood as the small influence that the slag surface thermal radiated power has on the pyrometer measurements of the other surfaces, an influence that decreases as the slag surface emissivity decreases.

The slag surface temperature correction in Figure 7 for the 0.5 and 0.3 emissivities is 14% and 36%, respectively. These corrections are large, but not as large as would be expected for an unenclosed heated surface. The analytical ray tracing and emissivity matrix method developed here can properly determine the correct temperature profile for one or more different surface emissivities within a furnace.

4. CONCLUSIONS

Our work with a dc arc furnace shows that temperature gradients exist inside a furnace for all operative regimes from warm up to processing. It is therefore important to correct pyrometer temperature measurements for the reflected component of the pyrometer field of view. A ray tracing and emissivity matrix analysis method as developed here is needed to determine this correction. The surface emissivity and the number of reflected bounces are the two key parameters in determining the precision and degree of correction. More surface bounce points need to be included in the analysis for surfaces with lower emissivity and higher temperatures. The resulting temperature correction is smaller than a straight forward correction for surface emissivity, as done with an unenclosed surface, but still significant.

The analytical method presented here for correcting pyrometer temperature profiles inside furnaces is very general and can be applied to any enclosed heated region. It can be expanded to include much larger data sets than used in the examples above, as well as to situations with nonuniform surface emissivity. All that is required is a well defined internal furnace geometry, raw temperature profile, and knowledge of the surface emissivities. With the availability of new pyrometer technology for scanning surface temperature profiles inside harsh furnace environments and having simultaneous capability for measurement of surface emissivity [7], this method will make possible the determination of temperatures with previously unavailable accuracies inside many manufacturing processes.

ACKNOWLEDGMENTS

The authors are very grateful to David Woolley for providing a program for estimating the bounce point locations and also thankful to David Rhee for computational assistance. This work was supported by Battelle Pacific Northwest National Laboratory as part of the Landfill Stabilization and Mixed Waste Focus Areas, Office of Technology Development, Environmental Management, U.S. Department of Energy.

REFERENCES

1. Munz, R. J. and Chen, G. Q., JNMM, Fall (1995) 32-37.
2. Mee, D. K., Lind, R. F., Bradley, N. C., Childs, R. M., Scott. K. J., and Tuker, Sr., R. W., Advances in Instrumentation, Proceedings v 45 pt 4, ISA Services Inc., Research Triangle Pk, NC, USA (1990) 2047-2064.
3. Cielo, P. Krapez, J. C., Lamontagne, Thomson, J. G., and Lamb, M. G.< Proceedings of SPIE v 1682 Thermosense XIV (1992) 142-154.
4. Nokes, B., Glass Industry, Nov. (1990) 13-14.
5. Visniauskas, V. V., Heat Transfer - Soviet Research, 22 (1990) 567-573.

6. Watanabe, T., Torii, T., Hirasawa, S., and Takagaki, T., IEEE Trans. on Semiconductor Manuf., 4 (1991) 59-63.

7. Woskov, P. P., Cohn, D. R., Rhee, D. Y., Thomas, P., Titus, C. H., Surma, J. E., Rev. Sci. Instrum., 61 (1995) 4241 - 4248.

8. Lee, S. K., "Accurate Pyrometry Inside an Arc Furnace by Taking Into Account the Surface Emissivity with a Ray-Tracing Analysis", SM Thesis, M.I.T., 1996.

9. Surma, J. E., Cohn, D. R., Smatlak, D. L., Thomas, P., Woskov, P. P., Titus, C. H., Wittle, J. K., and Hamilton, R. A., PNL-SA-21891, Pacific Northwest Laboratory, Richland, WA. 1993.

10. Woskov, P. P. and Titus, C. H., IEEE Trans. on Microwave Theory and Techniques, 43 (1995) 2684-2688.

11. Bekefi, G., Radiation Processes in Plasmas, John Wiley and Sons, New York, 1966, p. 46.

12. Oliver, B. M., Proc. IEEE, May (1965) 436-454.

13. Dicke, R. H., Beringer, R., Kyhl, R. L., and Vane, A. B., Phys. Rev. 70 (1946) 340-348.

Table 1. Mark II Temperature Profile Analysis for Two Bounce Treatment with One Emissivity

View Angle (°)	(r, z) First bounce point (cm)	Second bounce point	The measured temperatures in terms of actual temperatures
0	39.9, 109.2	39.9, 0	$T_0^m = \varepsilon T_0 + \varepsilon(1-\varepsilon)T_{180}$
10	37.6, 109.2	38.6, 0	$T_{10}^m = \varepsilon T_{10} + +0.615\varepsilon(1-\varepsilon)T_{160} + 0.385\varepsilon(1-\varepsilon)T_{180}$
20	36.8, 109.2	45.8, 35.9	$T_{20}^m = \varepsilon T_{20} + 0.485\varepsilon(1-\varepsilon)T_{120} + 0.515\varepsilon(1-\varepsilon)T_{130}$
30	38.1, 109.2	45.8, 78.9	$T_{30}^m = \varepsilon T_{30} + 0.671\varepsilon(1-\varepsilon)T_{70} + 0.329\varepsilon(1-\varepsilon)T_{80}$
40	42.4, 109.2	45.8, 101.8	$T_{40}^m = \varepsilon T_{40} + \varepsilon(1-\varepsilon)T_{50}$
50	45.7, 101.7	41, 109.2	$T_{50}^m = \varepsilon T_{50} + 0.325\varepsilon(1-\varepsilon)T_{30} + 0.675\varepsilon(1-\varepsilon)T_{40}$
60	45.7, 90.6	37.5, 109.2	$T_{60}^m = \varepsilon T_{60} + 0.48\varepsilon(1-\varepsilon)T_{20} + 0.52\varepsilon(1-\varepsilon)T_{30}$
70	45.7, 81.5	45.7, 101.3	$T_{70}^m = \varepsilon T_{70} + \varepsilon(1-\varepsilon)T_{50}$
80	45.7, 73.5	45.7, 83.1	$T_{80}^m = \varepsilon T_{80} + 0.198\varepsilon(1-\varepsilon)T_{60} + 0.802\varepsilon(1-\varepsilon)T_{70}$
90	45.7, 66.0	45.7, 66.0	$T_{90}^m = T_{90}$ by azimuthal symmetry
100	45.7, 58.5	45.7, 48.9	$T_{100}^m = \varepsilon T_{100} + 0.82\varepsilon(1-\varepsilon)T_{110} + 0.182\varepsilon(1-\varepsilon)T_{120}$
110	45.7, 50.6	45.7, 30.8	$T_{110}^m = \varepsilon T_{110} + 0.034\varepsilon(1-\varepsilon)T_{120} + 0.966\varepsilon(1-\varepsilon)T_{130}$
120	45.7, 41.5	45.7, 10.1	$T_{120}^m = \varepsilon T_{120} + 0.654\varepsilon(1-\varepsilon)T_{140} + 0.346\varepsilon(1-\varepsilon)T_{150}$
130	45.7, 30.4	37.9, 0	$T_{130}^m = \varepsilon T_{130} + 0.794\varepsilon(1-\varepsilon)T_{160} + 0.206\varepsilon(1-\varepsilon)T_{170}$
140	45.7, 15.5	39.4, 0	$T_{140}^m = \varepsilon T_{140} + 0.23\varepsilon(1-\varepsilon)T_{160} + +0.77\varepsilon(1-\varepsilon)T_{180}$
150	43.4, 0	45.7, 7.5	$T_{150}^m = \varepsilon(1.518 - 0.518\varepsilon)T_{150} + 0.482\varepsilon(1-\varepsilon)T_{140}$
160	37.9, 0	45.7, 50.6	$T_{160}^m = \varepsilon T_{160} + \varepsilon(1-\varepsilon)T_{110}$
170	37, 0	40.0, 109.2	$T_{170}^m = \varepsilon T_{170} + 1.087\varepsilon(1-\varepsilon)T_0 - 0.087\varepsilon(1-\varepsilon)T_{30}$
180	39.9, 0	39.9, 109.2	$T_{180}^m = \varepsilon T_{180} + \varepsilon(1-\varepsilon)T_0$

Note: Originally, $T_{150}^m = \varepsilon T_{150} + \varepsilon(1-\varepsilon)[0.518(T_{150} - T_{140}) + T_{140}]$

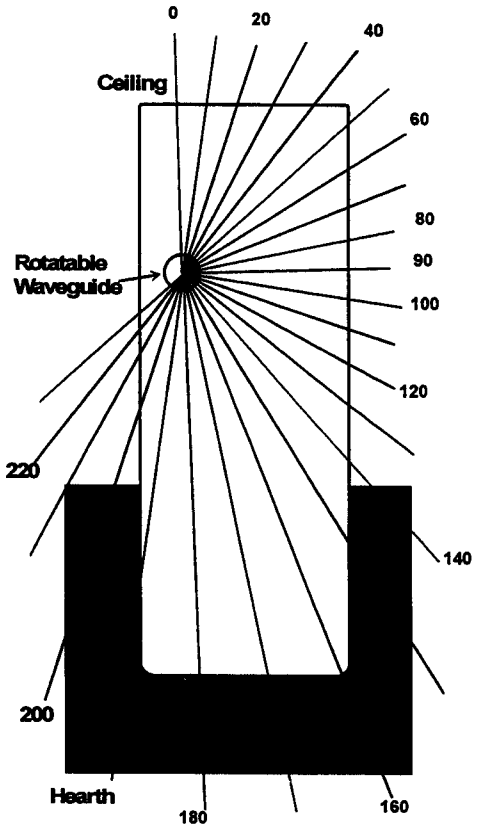

Fig. 1 Pyrometer View Angle inside the Mark II arc furnace.

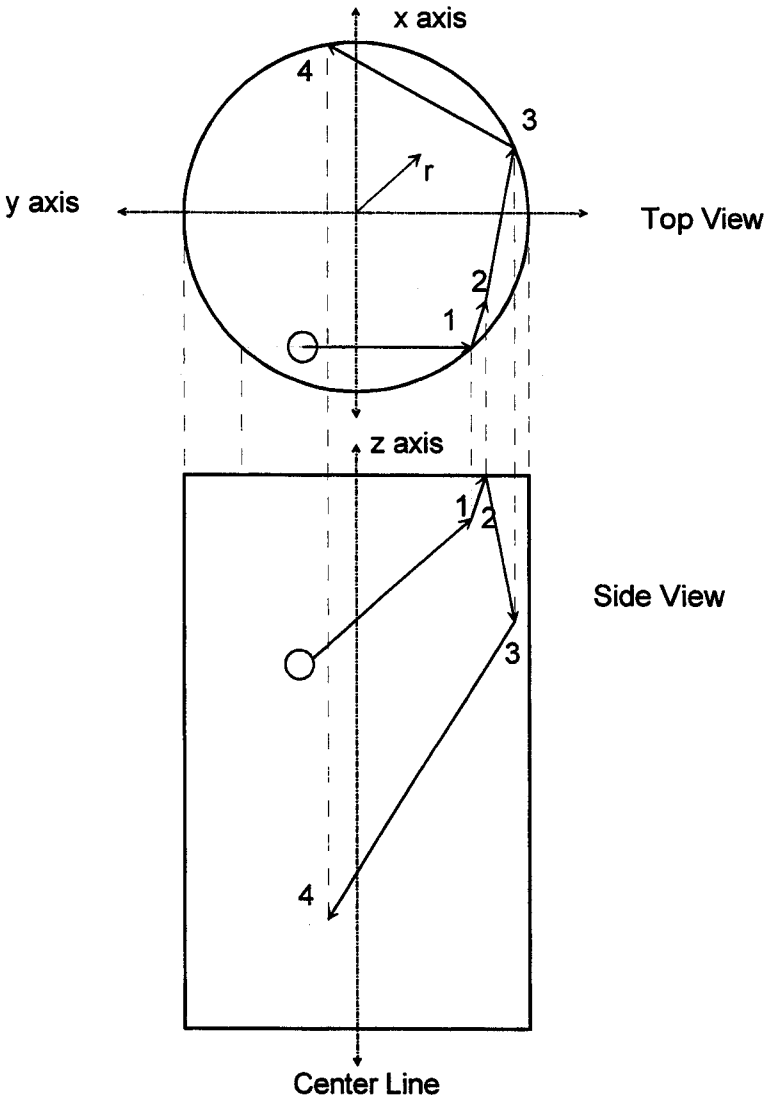

Bounce point 1 = (-36.8, -27.2, 101.7)

Bounce point 2 = (-28.1, -29.8, 109.2)

Bounce point 3 = (15.3, -43.1, 71.2)

Bounce point 4 = (45.7, 2.0, 25.5)

Fig. 2 Bounce point locations corresponding to 50° view angle

Note: The small circles represent the FOV launch mirror and coordinates (x, y, z) are expressed in centimeters

0.74	19 x 19 matrix																		RHS		Solution
0.74	0	0	0	0	0	0	0	0	0	0	0	0	0	0	0	0	0	0.19	1238		1272.36
0	0.74	0	0	0	0	0	0	0	0	0	0	0	0	0	0	0.12	0	0.07	1272		1323.05
0	0	0.74	0	0	0	0	0	0	0	0	0	0.09	0.1	0	0	0	0	0	1270		1347.26
0	0	0	0.74	0	0	0	0.13	0.06	0	0	0	0	0	0	0	0	0	0	1254		1345.92
0	0	0	0	0.74	0.19	0	0	0	0	0	0	0	0	0	0	0	0	0	1240		1341.31
0	0	0	0.06	0.13	0.74	0	0	0	0	0	0	0	0	0	0	0	0	0	1210		1286
0	0	0.09	0.1	0	0	0.74	0	0	0	0	0	0	0	0	0	0	0	0	1238		1322.87
0	0	0	0	0	0.19	0	0.74	0	0	0	0	0	0	0	0	0	0	0	1238		1338.61
0	0	0	0	0	0	0.04	0.15	0.74	0	0	0	0	0	0	0	0	0	0	1253		1346.01
0	0	0	0	0	0	0	0	0	1	0	0	0	0	0	0	0	0	0	1265		1265
0	0	0	0	0	0	0	0	0	0	0.74	0.16	0.04	0	0	0	0	0	0	1270		1358.21
0	0	0	0	0	0	0	0	0	0	0	0.74	0.01	0.19	0	0	0	0	0	1290		1370.9
0	0	0	0	0	0	0	0	0	0	0	0	0.74	0	0.13	0.07	0	0	0	1325		1404.2
0	0	0	0	0	0	0	0	0	0	0	0	0	0.74	0	0	0.15	0.04	0	1353		1433.08
0	0	0	0	0	0	0	0	0	0	0	0	0	0	0.74	0	0.04	0	0.15	1390		1479.54
0	0	0	0	0	0	0	0	0	0	0	0	0	0	0.09	0.84	0	0	0	1395		1497.97
0	0	0	0	0	0	0	0	0	0	0	0.19	0	0	0	0	0.74	0	0	1382		1511.13
0.21	0	0	-0	0	0	0	0	0	0	0	0	0	0	0	0	0	0.74	0	1395		1555.98
0.19	0	0	0	0	0	0	0	0	0	0	0	0	0	0	0	0	0	0.74	1385		1540.81

Fig. 3 Emissivity matrix by two bounce analysis with one emissivity applied to the high temperature set

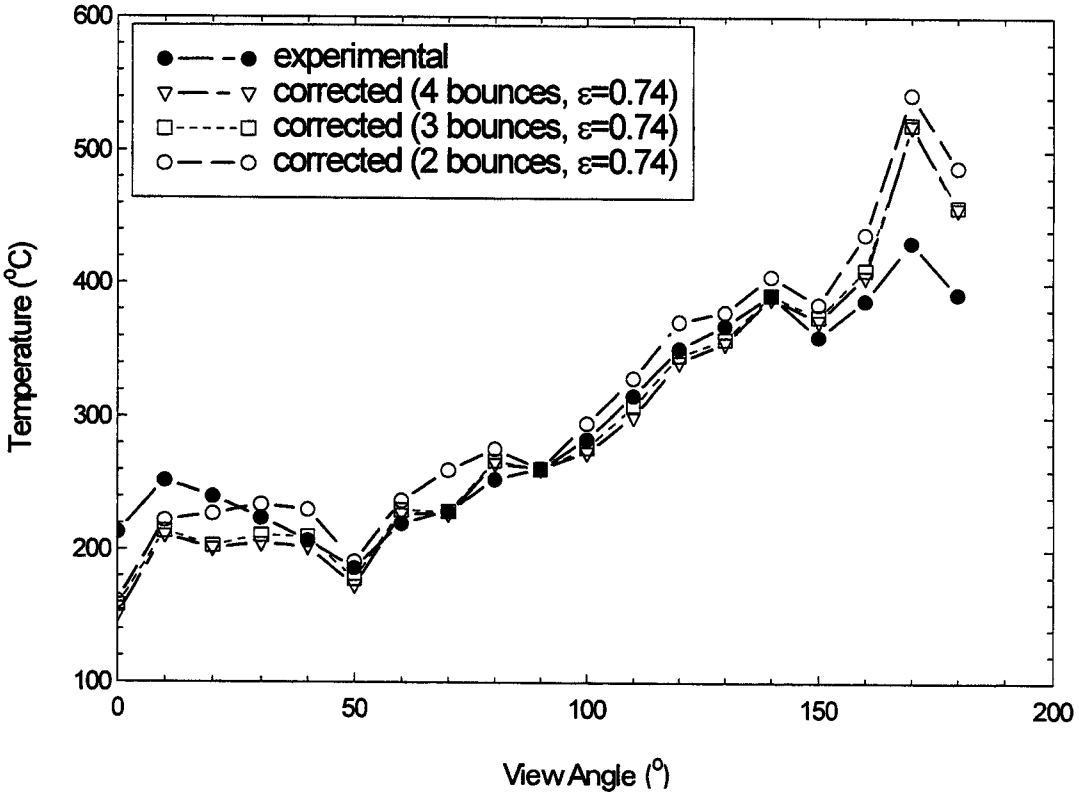

Fig. 4 Raw experimental and corrected temperature profiles for different assumptions on the number of FOV reflective bounces at low temperature inside Mark II.

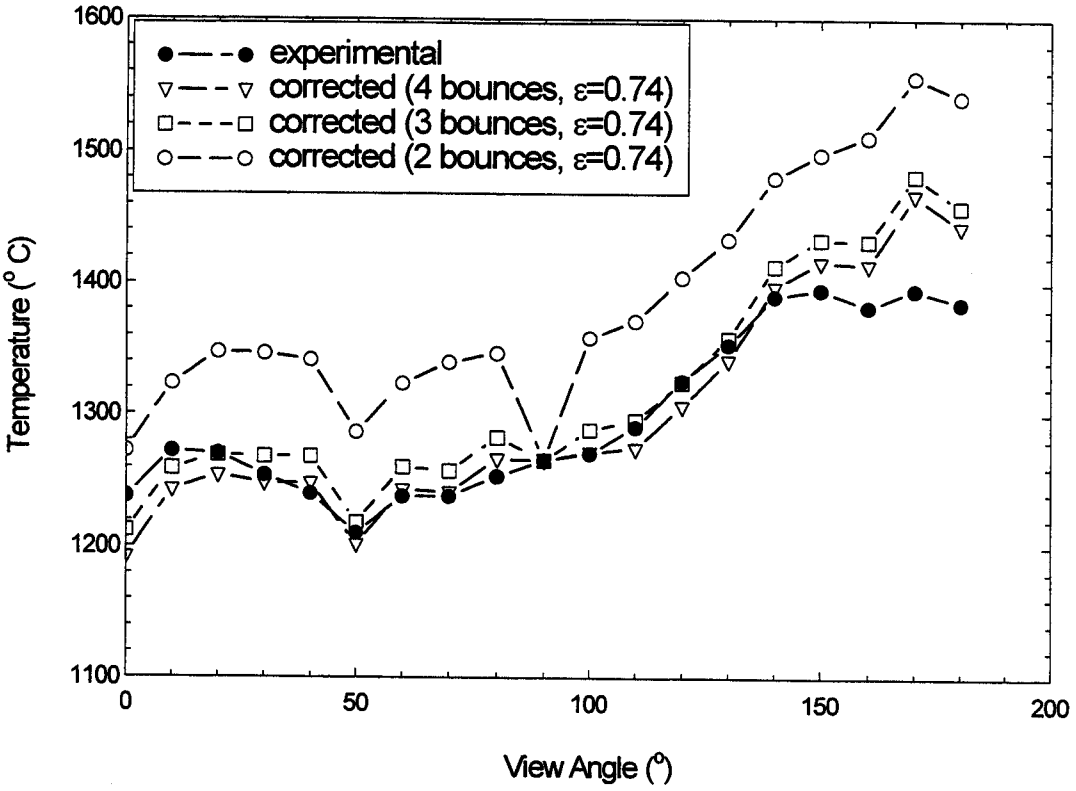

Fig. 5 Raw experimental and corrected temperature profiles for different assumptions on the number of FOV reflective bounces at high temperature inside Mark II.

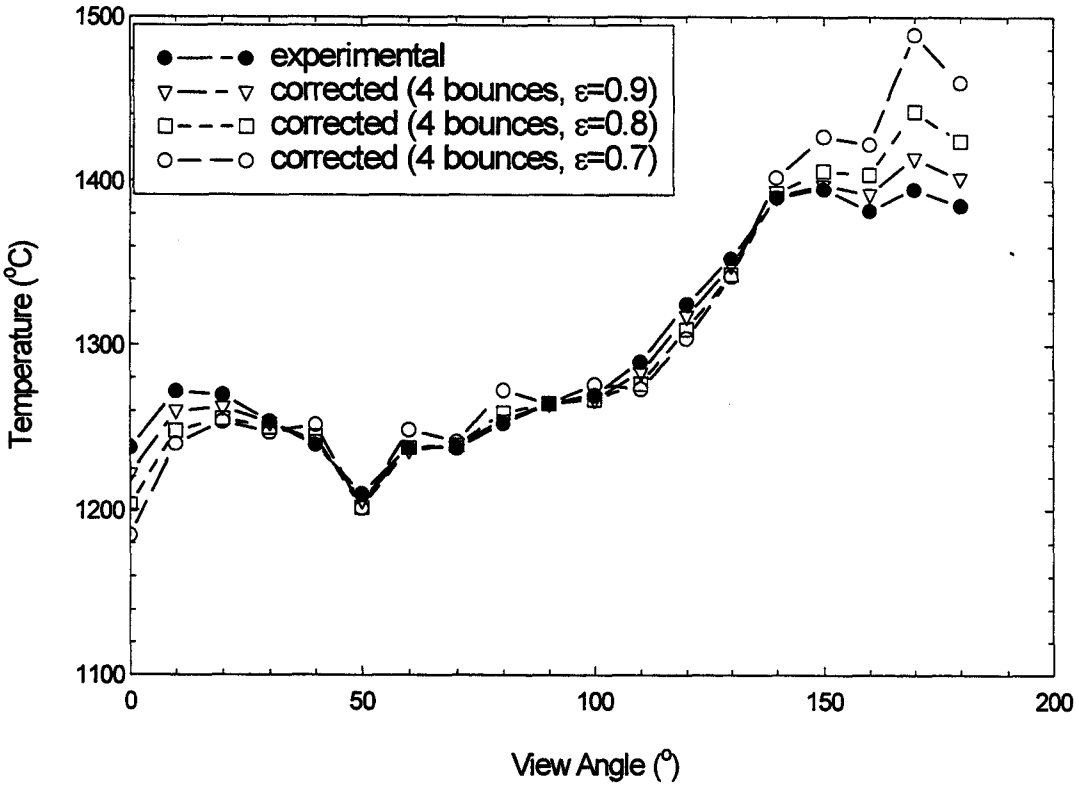

Fig. 6 Effect of different values for the uniform emissivity on the temperature correction with four FOV reflective bounces for the high temperature case.

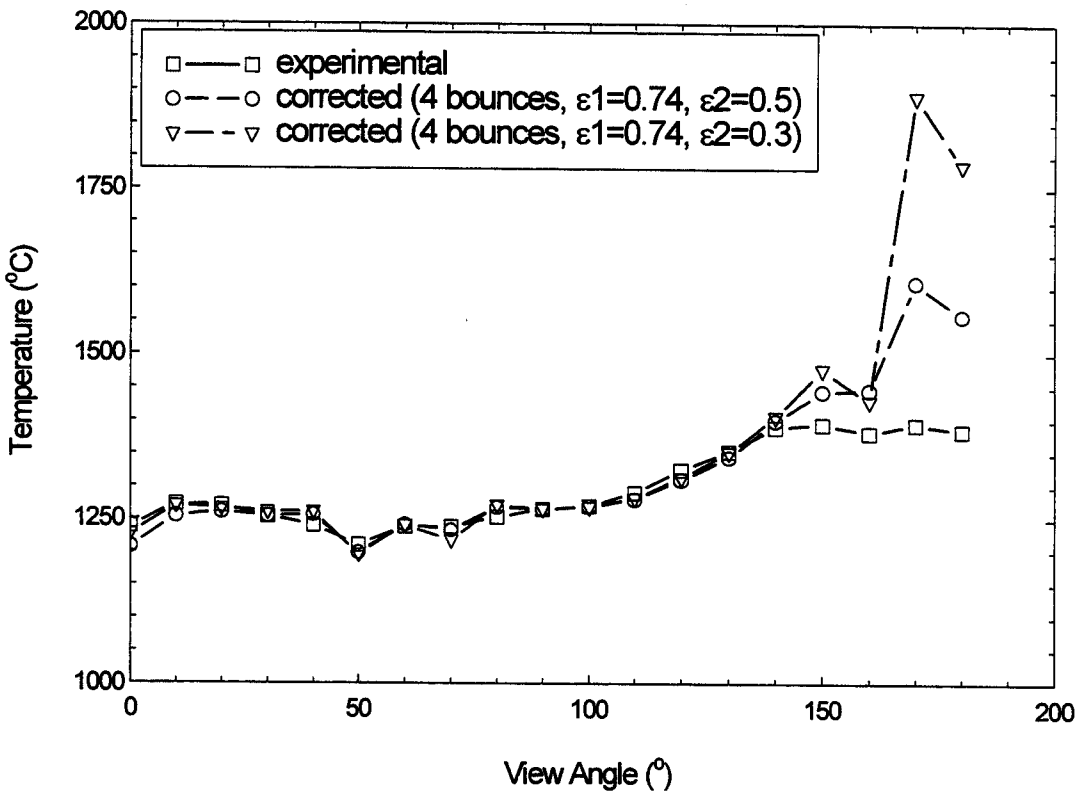

Fig. 7 Effect of a different lower slag surface emissivity on the temperature correction with four FOV reflective bounces at high temperature.